Both functions are closely related to colon cancer suppression (21). Although theoretical studies were performed to elucidate how LCA binds to $1,25(OH)_2D_3$, the agonistic mechanism of VDR by LCA was still unclear (18, 22).

Here we determined the crystal structures of the ligand binding domain (LBD) of rat VDR in ternary complexes with a synthetic peptide containing the target sequence of the coactivator MED1 (mediator of RNA polymerase II transcription subunit 1, also known as ARC205 and DRIP205) and the ligands LCA, 3-keto LCA, LCA acetate, and LCA propionate (**Fig. 1**) to investigate how LCA and its derivatives bind to VDR and how they act as the agonists. The structures reveal that LCA and its derivatives bind to the same ligand-binding pocket (LBP) of VDR that $1,25(OH)_2D_3$ binds to (23–31), but in the opposite orientation. Comparison of these structures also show how LCA and its derivatives mimic $1,25(OH)_2D_3$ and give insight into how the C-3 substituents on the A-ring affect the activity of each ligand. The structures also provide a sound basis for designing new compounds using the scaffold of LCA.

## MATERIALS AND METHODS

### Preparation of LCA ligands

LCA, 3-keto LCA, and LCA acetate were commercially obtained. LCA propionate was synthesized as follows. Boron trifluoride diethyl ether complex (44 μl, 0.33 mmol) was added to a stirred solution of LCA (504.5 mg, 1.34 mmol) in a mixture of propionic anhydride (1.67 ml) and tetrahydrofuran (5 ml) at 0°C, and the resulting solution was stirred at room temperature for 14.5 h. Aqueous sodium hydrogen carbonate was added to this solution, and the reaction mixture was stirred at room temperature for 1 h. Crude LCA propionate was extracted from the reaction mixture with ethyl acetate (AcOEt). The organic layer containing LCA propionate was washed with brine and dried over anhydrous magnesium sulfate, and the solvents were evaporated under house vacuum. The residue was purified by chromatography on silica gel (15 g) with 10% AcOEt/hexane to yield 460 mg (79%) of LCA propionate. The product was recrystallized on AcOEt/hexane.

### Protein expression, purification, and crystallization

Rat VDR-LBD (residues 116–423, Δ165–211) was expressed, purified, and crystallized as described by Vanhooke et al. and Nakabayashi et al. (31, 32). The purity and homogeneity of the protein was assessed by SDS-PAGE. The concentration of the protein was determined by UV absorption at 280 nm with molar extinction coefficients estimated using the method developed by Pace et al. (33). The 13mer synthetic oligopeptide (KNHPMLMNLLKDN), which corresponds to residues 625–637 of rat MED1, was purchased from World Gene Co., Ltd. (Tokyo, Japan). Each of the four ligands, LCA, 3-keto LCA, LCA acetate, and LCA propionate, was used to prepare a ternary complex of VDR-LBD/peptide/ligand in 10 mM Tris·HCl (pH 7.0), 10 mM dithiothreitol, and 0.02% sodium azide. All the ternary complexes were crystallized at 20°C in a series of precipitant solutions containing 0.1–0.4 M sodium formate, 12–22% (w/v) polyethylene glycol 4000, and 0–10% (v/v) ethylene glycol.

### X-ray diffraction data collection and structural analysis

The crystals were flash-frozen using mother liquor supplemented with 10% ethylene glycol. Diffraction data for the ternary complexes were collected at 95 K at beamline BL-6A at the Photon Factory of the High Energy Accelerator Research Organization and were integrated and scaled with HKL2000 (HKL Research, Inc.). The space group for each complex is *C*2; the unit cell dimensions are listed in **Table 1** with one complex per asymmetrical unit. The structures were solved by molecular replacement by using the crystal structure of the ternary complex reported by Vanhooke et al. (PDB code: 1RK3) as the search model in CNS (31, 34). Refinement was performed with CNS and XtalView (35).

## RESULTS

### Overall structures of the ternary complexes

The crystal structures of the ternary complexes of VDR-LBD with LCA and its three derivatives were determined at 1.9–2.2 Å resolution by X-ray crystallography (Table 1 and **Fig. 2A**). Most of the residues in the complexes were unambiguously determined; however, the N-terminal region (Ala116–Gln122), the middle region (Asp160–Gly164 and Ser212–Leu217), and the C-terminal end (Ser423) of

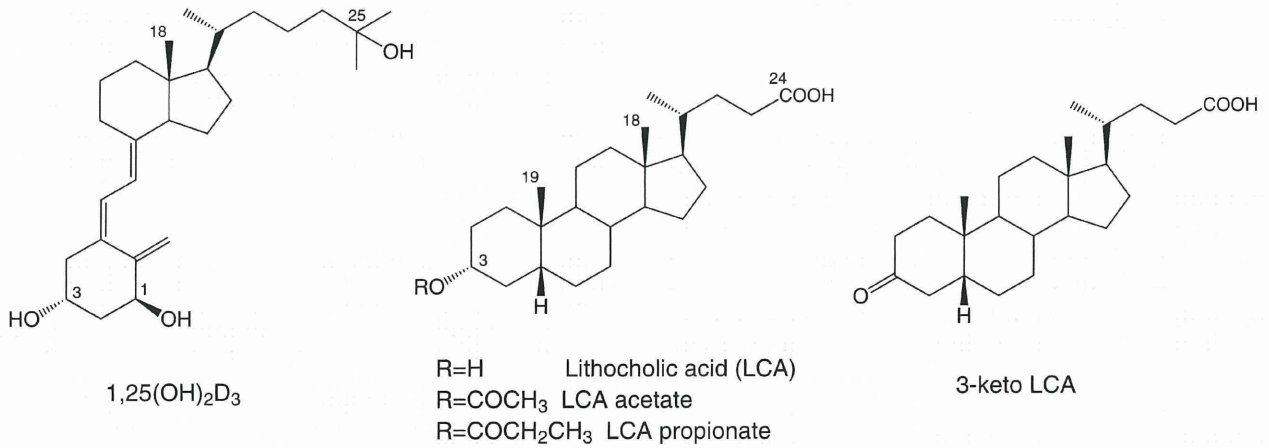


**Fig. 1.** Chemical structures of $1,25(OH)_2D_3$, LCA, and LCA derivatives.

TABLE 1. Data collection and refinement statistics

| Ligands | LCA | LCA Acetate | LCA Propionate | 3-keto LCA |
|---|---|---|---|---|
| Data collection | | | | |
| Unit cell dimensions | | | | |
| *a* (Å) | 154.5 | 154.4 | 154.5 | 153.8 |
| *b* (Å) | 42.4 | 42.0 | 42.8 | 42.3 |
| *c* (Å) | 41.6 | 41.5 | 41.6 | 41.5 |
| β (degree) | 96.8 | 96.2 | 96.3 | 96.4 |
| Resolution (Å) | 50–1.9 (1.96–1.90) | 50–2.2 (2.28–2.20) | 50–2.2 (2.28–2.20) | 50–1.9 (1.96–1.90) |
| Completeness (%) | 99.2 (99.9) | 99.3 (95.9) | 99.6 (96.8) | 99.2 (99.8) |
| Redundancy | 3.6 (3.6) | 4.3 (4.0) | 3.6 (3.4) | 3.6 (3.5) |
| I/σ(I) | 43.1 (6.2) | 26.2 (4.4) | 30.3 (3.9) | 41.3 (4.7) |
| $R_{sym}$ (%) | 3.2 (26.4) | 5.8 (29.5) | 4.5 (35.7) | 4.4 (32.9) |
| Refinement | | | | |
| R (%) | 23.3 | 22.0 | 21.1 | 23.4 |
| R-free (%) | 26.3 | 27.6 | 26.5 | 27.9 |
| RMSD bond lengths (Å) | 0.0058 | 0.0068 | 0.0069 | 0.0065 |
| RMSD bond angles (degree) | 1.25 | 1.19 | 1.18 | 1.22 |
| Number of atoms | | | | |
| Protein | 1925 | 1942 | 1942 | 1926 |
| Peptide | 92 | 92 | 92 | 92 |
| Ligand | 27 | 30 | 31 | 27 |
| Water | 108 | 49 | 56 | 110 |
| Average B factor (Å$^2$) | 41.0 | 50.1 | 49.9 | 43.8 |

VDR-LBD, and Asp636 and Asn637 of the MED1 peptide were not detected, probably due to fluctuation in these regions. Two more residues at the C-terminal end (Glu421 and Ile422) were also undetectable in the complexes with LCA and 3-keto LCA. Most of these missing residues were previously reported as invisible in studies of other ternary complexes of VDR and are likely a characteristic common to crystals of VDR complexes (23–31).

The overall structures of VDR-LBD in the four complexes are nearly identical (Fig. 2B). The root-mean-square deviations (RMSD) between the proteins in the LCA complex and each of the 3-keto LCA, LCA acetate, and LCA propionate complexes are 0.34, 0.52, and 0.52 Å, respectively, using the Cα atoms of Lys123–Met159 and Ser218–Asn420. Furthermore, the RMSD between the proteins in the LCA and 1,25(OH)$_2$D$_3$ complexes is 0.49 Å for the overall structure (Fig. 2C). Therefore, no significant structural differences were found among the proteins in the ternary complexes with LCA, its derivatives, or 1,25(OH)$_2$D$_3$ (28, 31).

### Structures of the ligands and their interactions with VDR-LDB

Proteins in the NR super family have a common ligand-binding pocket (LBP). Residues in helices 1, 3, 5, 11, and 12, all β-turns, and loops 6–7 and 11–12 form the framework for the LBP of VDR. The natural hormone 1,25(OH)$_2$D$_3$ is accommodated in the LBP. In the present study, we observed clear electron density in the LBP, as was previously reported in the complex with 1,25(OH)$_2$D$_3$ (**Fig. 3A**) (28), and crystallographic refinement allowed us unambiguous determination of the structure of LCA and its derivatives in the complex (Figs. 2A and 3A).

Except for their respective substituents, LCA and its three derivatives are accommodated in the LBP of VDR-LBD with almost identical structures. However, their orientation

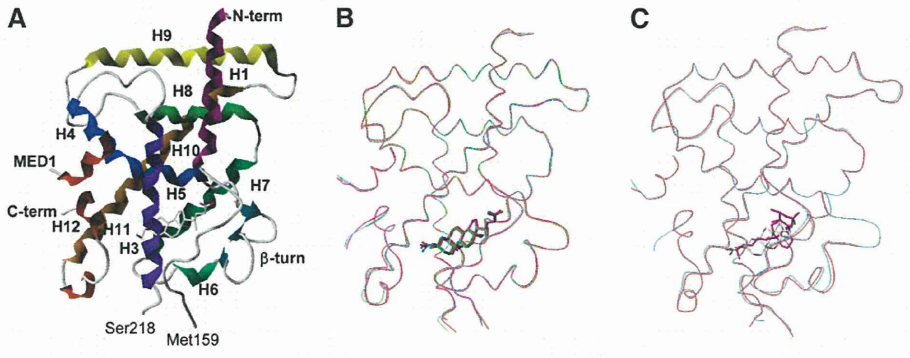


**Fig. 2.** Overall structures of ternary complexes of VDR with LCA derivatives. A: Complex structure of VDR with LCA. VDR and MED1 are represented by ribbons, and LCA is represented by a stick. The helices of VDR are numbered after that of the human RXR. B: Superposition of Cα traces of the four ternary complexes of VDR with LCA derivatives. Complexes with LCA, 3-keto LCA, LCA acetate, and LCA propionate are represented in red, green, cyan, and magenta, respectively. C: Superposition of Cα trace of ternary complexes of VDR with LCA (cyan) and 1,25(OH)$_2$D$_3$ (red) complex.

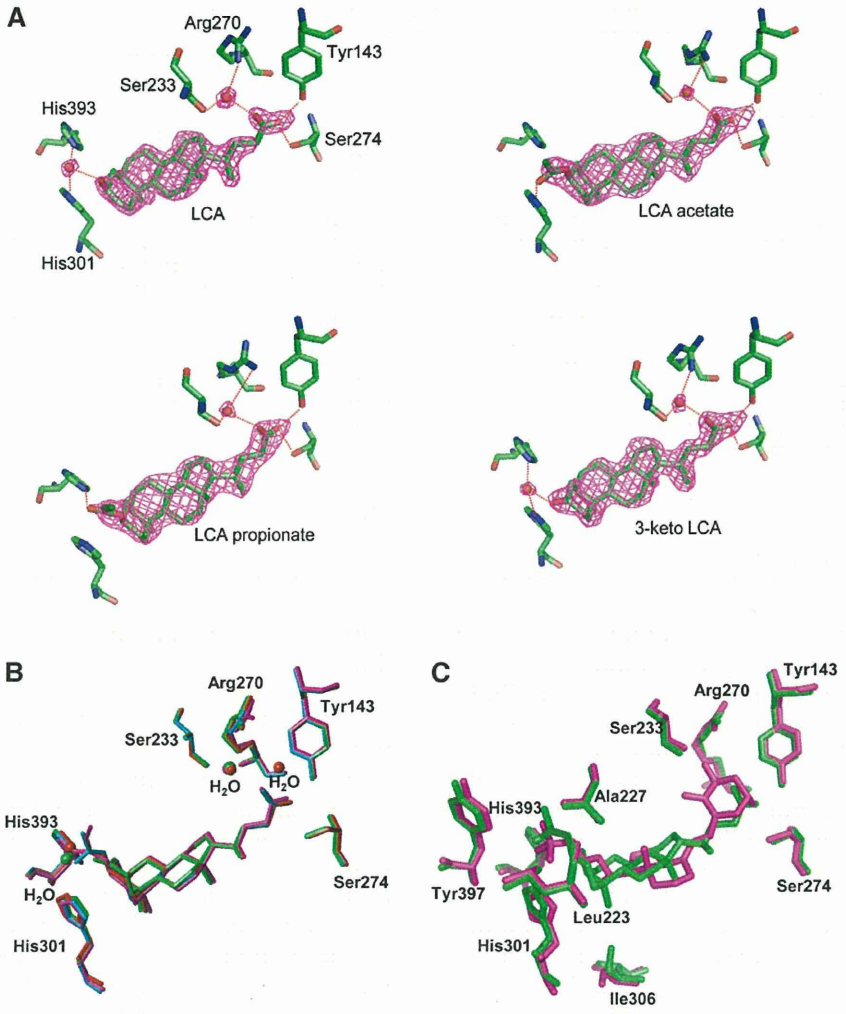


**Fig. 3.** A: Hydrogen-bonding network between VDR and LCA derivatives, LCA, 3-keto LCA, LCA acetate, and LCA propionate. The purple fishnet is the $F_o$-$F_c$ omit-annealed difference Fourier electron-density map contoured at 3σ level from the average of the map. The oxygen atoms of water are represented by red spheres. B: Superposition of the four LCA derivatives in VDR complexes. LCA, 3-keto LCA, LCA acetate, and LCA propionate are represented in red, green, cyan, and magenta, respectively. C: Superposition of LCA acetate (green) and $1,25(OH)_2D_3$ (magenta) in VDR complexes.

is opposite to that of $1,25(OH)_2D_3$ in both the horizontal and vertical planes (Fig. 3C). The 24-carboxyl group is directed toward the β-turns, and the β-face of the steroid is directed toward helix 7 in the bottom of the LBP, while the A-ring faces helix 12 (Fig. 2A). LCA forms three hydrogen bonds at the carboxyl group. One oxygen atom of the carboxyl group directly forms hydrogen bonds with the hydroxyl groups in the side chains of Tyr143 in helix 1 (the distance between the oxygen atoms of the carboxyl group and the hydroxyl group is 2.46 Å) and Ser274 in helices 4/5 (the distance between the oxygen atoms of the carboxyl group and the hydroxyl group is 2.76 Å). The other oxygen atom of the same carboxyl group interacts via a water molecule (the distance between the oxygen atoms of the water and the carboxyl group is 2.69 Å), with the hydroxyl group in the side chain of Ser233 in helix 3 and the guanidinium group in the side chain of Arg270 in helix 4/5 (the distance between the water molecule and these residues are 2.92 Å and 3.01 Å, respectively) (Fig. 3A). These hydrogen bonds are also observed in the other three complexes. The four rings of the steroid in each of the complexes interact with hydrophobic residues in the LBP through hydrophobic interactions. There are 12 residues (Leu226, Leu229, Val230, Ile264, Ile276, Met268, Trp282, Val296, Ala299, Leu305, Ile306, and Leu309) distributed within 4.3 Å from the rings. Such hydrophobic interactions are also conserved in the other complexes.

Hydrogen bonds between VDR and the ligands are also observed at the other end of the ligands, the C-3 position of the A-ring. The four ligands differ in their substituents at this position. The hydroxyl group of LCA, the carbonyl group of 3-keto LCA, the propionyl group of LCA propionate, and the acetyl group of LCA acetate interact with residues in helix 6, loop 6–7, and helix 11 (Figs. 2A and 3A). In the

complexes with LCA and 3-keto LCA, the oxygen atoms of the respective hydroxyl and carbonyl groups of the substituents interact via a water-mediated hydrogen bond with the nitrogen atoms of imidazole rings of His301 in helix 6 and His393 in helix 11. In contrast, in the complex with LCA acetate, the oxygen atom of the acetyl group directly forms a hydrogen bond with the nitrogen atom of the imidazole ring of His301. In the complex with LCA propionate, the oxygen atom of the propionyl group also directly forms a hydrogen bond with the nitrogen atom of the imidazole ring of His393. Furthermore, the alkyl parts of the two substituents interact with the aromatic rings of Tyr397 in helix 11 and Phe418 in helix 12 and with the side chains of Leu410 and Val414 in helix 12, stabilizing the binding of the two derivatives to the LBP of VDR-LBD (Fig. 3A). From this viewpoint, LCA propionate may be the most effective of the four ligands because it has the longest alkyl part in the substituent.

### Structure of the MED1 peptide

NR super family proteins generally include two domains for two types of transactivations, a constitutive activation function (AF-1) and a ligand-dependent activation function (AF-2). The AF-2 domain of the VDR-LBD consists of helices 3, 4, and 12, and loop 3–4, and it interacts with the LXXLL motif known as the NR-box. In the present study, we synthesized a peptide containing the target sequence of the MED1 coactivator and determined the structure of the peptide in the four ternary complexes to investigate whether or not LCA and its derivatives affect coactivator binding. The peptide binds to the AF-2 domain in each of the four complexes similar to the complex with $1,25(OH)_2D_3$. Although two residues of the peptide, Asp636 and Asn637, have no detectable structure as described above, the rest of the peptide forms an α-helix with a kink at Pro628 in each complex (**Fig. 4A**). The structure of the peptide in the four complexes is nearly identical. The RMSDs between the peptides in the LCA complex and the 3-keto LCA, LCA acetate, and LCA propionate complexes are 0.22, 0.58, and 0.69 Å, respectively, using the Cα atoms of Lys625–Lys635. The structure of the peptide in the LCA complex was also compared with that in the $1,25(OH)_2D_3$ complex. The RMSD between the two peptides was calculated at 0.76 Å, indicating no significant structural differences among the peptides in the ternary complexes with LCA, its derivatives, and $1,25(OH)_2D_3$ (Fig. 4B) (28, 31).

The AF-2 domain forms a shallow pit consisting of five hydrophobic residues: Ile238 in helix 3, Ile256 in helix 4/5, Leu259 in helix 4/5, Leu413 in helix 12, and Val417 in helix 12. The peptide binds to this pit through the hydrophobic interactions between the LXXLL motif of the peptide and the complementary pit of the protein. The polar side chains of Lys242 in helix 3 and Glu416 in helix 12 also facilitate the binding of the peptide by clamping it on the both edges of the AF-2 domain (a charge clamping). Two hydrogen bonds are formed between the oxygen atom of the side chain carboxyl group of Glu416 and the amide nitrogen of Met629, and the nitrogen atom of the side chain amino group of Lys242 and the carbonyl oxygen of Leu633. All these interactions observed in the present study are the same as those seen in the complex with $1,25(OH)_2D_3$. Therefore, these results indicate that the interactions between the coactivator MED1 and the AF-2 domain are well conserved in the ternary complexes with LCA and its derivatives.

## DISCUSSION

Since the discovery of its function as an agonist of VDR, LCA has been expected to be used a vitamin D alternative, especially because LCA appears to activate VDR without causing hypercalcemia. However, because the functional mechanism of LCA was still unclear, LCA derivatives with higher activities have been found mainly by trial and error. In the present study, we determined the structures of ternary complexes of VDR-LBD with LCA and its derivatives and elucidated how they bind to VRD-LDB.

LCA and its derivatives bind to the same LBP that $1,25(OH)_2D_3$ binds to. However, their orientation is opposite to that of $1,25(OH)_2D_3$ (Fig. 3C). Its A-ring was set on the inlet of the LBP, while its 24-carboxyl group wedged

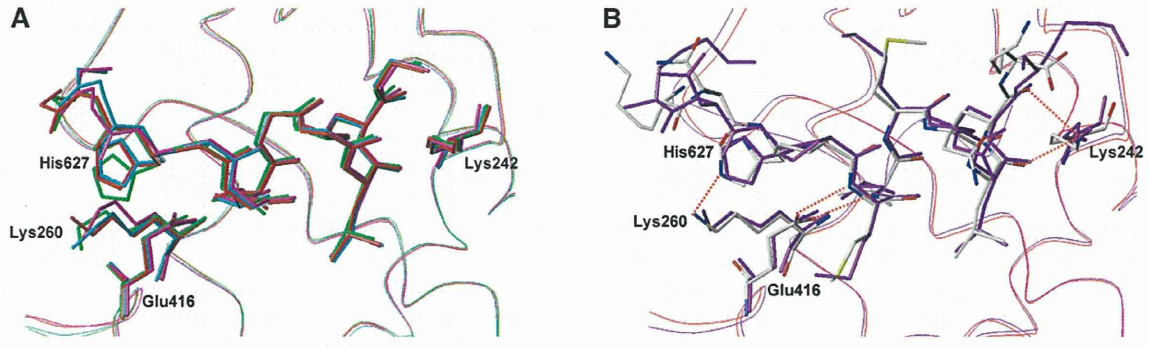


**Fig. 4.** Structures of MED1 peptides in VDR complexes. MED1 peptide and Lys242 and Glu416 of each VDR complex are represented by sticks; the other parts are represented by ribbons. A: Superposition of MED1 peptides in VDR complexes with LCA (red), 3-keto LCA (green), LCA acetate (cyan), and LCA propionate (magenta). B: Superposition of MED1 peptides in VDR complexes with LCA (magenta) and $1,25(OH)_2D_3$ (white carbons).

itself into the LBP. Interestingly this orientation is the same as that of 6α-ethyl-chenodeoxycholic acid (6α-ethyl-CDCA) in the farnesoid X receptor (FXR) (36). LCA and its derivatives are similar in size (14–16 Å × 5 Å × 3 Å; length × width × thickness) to natural $1,25(OH)_2D_3$ (approximately 15 Å × 5 Å × 2 Å), and although their shapes are somewhat different, the nonplanar *cis* A/B rings of the steroid scaffold of LCA mimic the curvature of the 9,10-secosteriod portion of $1,25(OH)_2D_3$ (Fig. 3C). Often, the size seems to be critical to the agonistic activity of a ligand. Agonistic ligands induce a conformational change of loop 11–12 to bring helix 12 into the active conformation, which is stabilized by hydrophobic interactions between the ligand and Val418 and Phe422 (Val414 and Phe418 of rat VDR, respectively). This conformation creates the AF-2 surface and allows the coactivator to bind, which is required for the VDR activity. Large ligands could collide with helix 12 and destabilize the active conformation. Indeed, several larger ligands have been reported to show antagonistic activity instead of agonistic activity (32, 37).

Despite their opposite orientation, LCA and its derivatives can reproduce the interactions between VDR and $1,25(OH)_2D_3$, which consists of a hydrophobic secosteroid framework and three polar groups. The polar groups are located at the both ends of the ligand and stabilize ligand binding through several hydrogen bonds, while the hydrophobic secosteroid frame just fits the hydrophobic tunnel of the LBP. In the complex with $1,25(OH)_2D_3$, the A-ring of $1,25(OH)_2D_3$ deeply wedges itself into the LBP and its 25-hydroxyl group is set on the inlet of the LBP. There are two polar groups at the C-1 and C-3 positions of the A-ring of $1,25(OH)_2D_3$, whose oxygen atoms form two pairs of bifurcated hydrogen bonds with the side chains of Tyr143 and Ser274, and Ser233 and Arg270, respectively. Furthermore, the 25-hydroxyl group of $1,25(OH)_2D_3$ also forms a bifurcated hydrogen bond with the nitrogen atoms of the imidazole rings of His301 and His393. In contrast, LCA and its derivatives consist of the hydrophobic steroid framework and two polar groups at the both ends (Fig. 1). However, they maintain most of the hydrogen bonds between the ligand and the protein by exchanging the hydrogen-bonding partners between the A-ring and the carboxyl group. Two oxygen atoms of the 24-carboxyl group form, with the help of a water molecule, two pairs of bifurcated hydrogen bonds directly with the side chains of Tyr143 and Ser274, and indirectly with Ser233 and Arg270, respectively. The hydrogen bonds with the nitrogen atoms of the imidazole rings of His301 and His393 are partially formed, depending on the substituents at the C-3 position of the A-ring. Therefore, the hydrogen-bonding network between the ligand and the protein is essentially the same for both LCA and $1,25(OH)_2D_3$, even though their orientations are opposite. Adachi et al. also indicated the importance of the hydrogen-bonding network for agonistic activity by showing that esterification of the carboxyl group of LCA weakened its agonistic activity (18).

Although LCA mimicked the dimensions and chemical properties of $1,25(OH)_2D_3$ as discussed above, its affinity is much lower than $1,25(OH)_2D_3$. In a competitive binding assay using VDR fused to glutathione *S*-transferase, $IC_{50}$ values were estimated as 0.08 nM and 300 μM for $1,25(OH)_2D_3$ and LCA, respectively (19). As the accessible surface areas of the hydrophobic surface of LCA and $1,25(OH)_2D_3$ are 371 $Å^2$ and 442 $Å^2$, respectively, the total hydrophobic interaction of LCA with VDR would be expected to be smaller than that of $1,25(OH)_2D_3$. Also the simple difference of the size between LCA ($C_{24}H_{40}O_3$) and $1,25(OH)_2D_3$ ($C_{27}H_{44}O_3$) suggests that the LBP accommodates LCA somewhat loosely. Such a feature allows several water molecules to penetrate the LBP of VDR. One of the water molecules is involved in the hydrogen bond network around the 24-carboxyl group. Another water molecule is incorporated in the hydrogen bond network around the C-3 position of the A-ring in the complex with LCA. However, given the affinity analyses mentioned above, the interactions mediated by hydrogen bonding seem to be less important for stabilizing the complex than the hydrophobic interactions.

The substituents at the C-3 position of the A-ring of LCA also affect the activation of human VDR, and LCA acetate and LCA propionate are more potent agonists than LCA and 3-keto LCA (18, 19, 22, 38). The biding assay mentioned above showed that $IC_{50}$ values for LCA acetate and LCA propionate are 30 μM, about 10 times more potent than LCA (19). Another cotransfection assay showed LCA acetate ($EC_{50}$ = 0.40 μM) is about 30 times more effective than LCA ($EC_{50}$ = 12.1 μM), whereas 3-keto LCA ($EC_{50}$ = 6.8 μM) is comparable to LCA (18). Our crystal structures show that the C-3 substituents of the former derivatives interact directly with VDR via a hydrogen bond, while the latter ones require a water molecule to form indirect hydrogen bonds with VDR. In addition, the alkyl part of these acyl groups interacts with the hydrophobic residues of VDR, including Val418 and Phe422 (Val414 and Phe418 of rat VDR, respectively), which are key residues in the VDR activation mechanism described above. These interactions are probably the reason for the higher potency of these two ligands because this valine is not directly involved in the interaction with the ligands in the case of LCA and 3-keto LCA. These additional interactions at the C-3 position may also explain some of the mutation analyses; the human VDR-S275A and S278A mutations (corresponding to S271A and S274A of rat VDR, respectively) almost completely abolished the activity of LCA, whereas they were still activated by LCA acetate (18). The extra interactions at the C-3 position compensate for the loss of the hydrogen bond due to the mutation to some extent.

Some of the other results from the mutation analyses could also be explained from our structure (18, 19, 22, 38). The VDR-S237M mutant (S233M of rat VDR) can respond to LCA but not to $1,25(OH)_2D_3$. The serine residue is directly interacts with the A-ring of $1,25(OH)_2D_3$ through a hydrogen bond, and the mutation to methionine would not only lose the capability of the interaction but also hinder the ligand binding. On the other hand, the bulky A-ring is replaced by a linear alkyl group in LCA (Fig. 3C), creating enough room to accommodate in the methionine. In contrast, the VDR-S278V mutant (S274V of rat VDR) is

activated by $1,25(OH)_2D_3$ but not by LCA. The side chain of the serine also directly interacts with the hydroxyl group of the A-ring of $1,25(OH)_2D_3$ and the carboxyl group of LCA. The mutation to valine would lose the hydrogen bond, but there is enough room to accommodate the replaced side chain in both cases. LCA might disfavor the mutant that would bring the hydrophobic valine close to the negative charge of the carboxyl group.

The role of His305 (His301 of rat VDR) in the interactions with the LCA-related ligands seems more complicated. Although LCA and 3-keto LCA interact with His305 in a very similar manner (Fig. 3A), the VDR-H305A (H301A of rat VDR) mutant significantly diminishes the LCA activity but has little effect on activation by LCA acetate or 3-keto LCA. The indole ring lies almost parallel to the A-ring of LCA, making van der Waals contacts. It is also involved in the hydrogen bond directly (LCA acetate) or indirectly (LCA and 3-keto LCA). These interactions are almost the only interactions between the ligand and loop 6–7, and the mutation to alanine may perhaps trigger a large conformational change of the loop, which could even expose the ligand to the solvent.

Although LCA activates VDR, it functions differently from $1,25(OH)_2D_3$; for example, it does not induce hypercalcemia. The most prominent difference in the ligand binding between $1,25(OH)_2D_3$ and the LCA-related ligands reported here are the pattern of the hydrogen bonds with Ser233 in helix 3 and Arg270 in helix 4/5. While 1α-hydroxyl group of $1,25(OH)_2D_3$ directly forms the hydrogen bonds with these two residues, all the LCA-related ligands studied here require a water molecule to form indirect hydrogen bonds with them, which is likely to weaken the interaction with VDR. Also, replacing the A-ring of $1,25(OH)_2D_3$ with a linear alkyl group seems to loosen the hydrophobic interactions around it, as highlighted by the VDR-S237M mutant discussed above. These differences may affect the structure of the AF-2 surface and, therefore, the interactions between VDR and the coactivators statically and/or dynamically.

However, we did not detect significant differences in the interactions between VDR and the coactivator peptide. One possible reason is the crystal packing. The coactivator peptide not only interacts with VDR but also plays an important role in the crystal packing, and even antagonists could be trapped in its active form at high concentrations as in the crystallization conditions (32). Thus the structural differences that may be caused by LCA could have been suppressed by the crystal packing. The possibility that LCA behaves differently from $1,25(OH)_2D_3$ through a nonstructural mechanism also cannot be excluded. Their metabolic behavior and/or cellular distribution would be different in vivo, causing the functional differences. To rationally elucidate the underlying reason for the difference in the agonistic activity between the ligands, it will be necessary to analyze the higher-ordered complexes, perhaps using full-length VDR. The crystal structures reported here nonetheless have shown the similarities and differences between LCA-related ligands and $1,25(OH)_2D_3$ in their interactions with VDR and should provide a sound basis for the design of new ligands based on LCA, hopefully with better pharmaceutical features.

### Data deposition

The coordinates of the determined structures have been deposited in the Protein Data Bank with accession numbers 3W5P, 3W5Q, 3W5R, and 3W5T for the LCA, 3keto-LCA, LCA acetate, and LCA propionate complexes, respectively.

The authors thank Professor H. Kagechika and Professor H. Tamamura of Tokyo Medical and Dental University for supporting this research project. The authors also thank the technical staff at the Photon Factory of the High Energy Accelerator Research Organization for maintenance of the beam line.

## REFERENCES

1. Haussler, M. R., G. K. Whitfield, C. A. Haussler, J. C. Hsieh, P. D. Thompson, S. H. Selznick, C. E. Dominguez, and P. W. Jurutka. 1998. The nuclear vitamin D receptor: biological and molecular regulatory properties revealed. *J. Bone Miner. Res.* **13:** 325–349.
2. Abe, E., C. Miyaura, H. Sakagami, M. Takeda, K. Konno, T. Yamazaki, S. Yoshiki, and T. Suda. 1981. Differentiation of mouse myeloid leukemia cells induced by 1 alpha,25-dihydroxyvitamin D3. *Proc. Natl. Acad. Sci. USA.* **78:** 4990–4994.
3. DeLuca, H. F. 2004. Overview of general physiologic features and functions of vitamin D. *Am. J. Clin. Nutr.* **80(Suppl.):** 1689–1696.
4. Hosomi, J., J. Hosoi, E. Abe, T. Suda, and T. Kuroki. 1983. Regulation of terminal differentiation of cultured mouse epidermal cells by 1 alpha,25-dihydroxyvitamin D3. *Endocrinology.* **113:** 1950–1957.
5. Lemire, J. M. 1992. Immunomodulatory role of 1,25-dihydroxyvitamin D3. *J. Cell. Biochem.* **49:** 26–31.
6. Smith, E. L., N. C. Walworth, and M. F. Holick. 1986. Effect of 1 alpha,25-dihydroxyvitamin D3 on the morphologic and biochemical differentiation of cultured human epidermal keratinocytes grown in serum-free conditions. *J. Invest. Dermatol.* **86:** 709–714.
7. Tanaka, H., E. Abe, C. Miyaura, T. Kuribayashi, K. Konno, Y. Nishii, and T. Suda. 1982. 1 alpha,25-Dihydroxycholecalciferol and a human myeloid leukaemia cell line (HL-60). *Biochem. J.* **204:** 713–719.
8. Bortman, P., M. A. Folgueira, M. L. Katayama, I. M. Snitcovsky, and M. M. Brentani. 2002. Antiproliferative effects of 1,25-dihydroxyvitamin D3 on breast cells: a mini review. *Braz. J. Med. Biol. Res.* **35:** 1–9.
9. Fraser, D., S. W. Kooh, H. P. Kind, M. F. Holick, Y. Tanaka, and H. F. DeLuca. 1973. Pathogenesis of hereditary vitamin-D-dependent rickets. An inborn error of vitamin D metabolism involving defective conversion of 25-hydroxyvitamin D to 1 alpha,25-dihydroxyvitamin D. *N. Engl. J. Med.* **289:** 817–822.
10. Glorieux, F. H., P. J. Marie, J. M. Pettifor, and E. E. Delvin. 1980. Bone response to phosphate salts, ergocalciferol, and calcitriol in hypophosphatemic vitamin D-resistant rickets. *N. Engl. J. Med.* **303:** 1023–1031.
11. Hayes, C. E. 2000. Vitamin D: a natural inhibitor of multiple sclerosis. *Proc. Nutr. Soc.* **59:** 531–535.
12. Konety, B. R., and R. H. Getzenberg. 2002. Vitamin D and prostate cancer. *Urol. Clin. North Am.* **29:** 95–106, ix.
13. Lamberg-Allardt, C. 1991. Is there a role for vitamin D in osteoporosis? *Calcif. Tissue Int.* **49(Suppl.):** S46–S49.
14. Langner, A., H. Verjans, V. Stapor, M. Mol, and M. Fraczykowska. 1993. Topical calcitriol in the treatment of chronic plaque psoriasis: a double-blind study. *Br. J. Dermatol.* **128:** 566–571.
15. Yamada, S., M. Shimizu, and K. Yamamoto. 2003. Vitamin D receptor. *Endocr. Dev.* **6:** 50–68.
16. Bouillon, R., W. H. Okamura, and A. W. Norman. 1995. Structure-function relationships in the vitamin D endocrine system. *Endocr. Rev.* **16:** 200–257.
17. Boehm, M. F., P. Fitzgerald, A. Zou, M. G. Elgort, E. D. Bischoff, L. Mere, D. E. Mais, R. P. Bissonnette, R. A. Heyman, A. M. Nadzan, et al. 1999. Novel nonsecosteroidal vitamin D mimics exert

VDR-modulating activities with less calcium mobilization than 1,25-dihydroxyvitamin D3. *Chem. Biol.* **6:** 265–275.
18. Adachi, R., Y. Honma, H. Masuno, K. Kawana, I. Shimomura, S. Yamada, and M. Makishima. 2005. Selective activation of vitamin D receptor by lithocholic acid acetate, a bile acid derivative. *J. Lipid Res.* **46:** 46–57.
19. Ishizawa, M., M. Matsunawa, R. Adachi, S. Uno, K. Ikeda, H. Masuno, M. Shimizu, K. Iwasaki, S. Yamada, and M. Makishima. 2008. Lithocholic acid derivatives act as selective vitamin D receptor modulators without inducing hypercalcemia. *J. Lipid Res.* **49:** 763–772.
20. Makishima, M., T. T. Lu, W. Xie, G. K. Whitfield, H. Domoto, R. M. Evans, M. R. Haussler, and D. J. Mangelsdorf. 2002. Vitamin D receptor as an intestinal bile acid sensor. *Science.* **296:** 1313–1316.
21. Degirolamo, C., S. Modica, G. Palasciano, and A. Moschetta. 2011. Bile acids and colon cancer: solving the puzzle with nuclear receptors. *Trends Mol. Med.* **17:** 564–572.
22. Choi, M., K. Yamamoto, T. Itoh, M. Makishima, D. J. Mangelsdorf, D. Moras, H. F. DeLuca, and S. Yamada. 2003. Interaction between vitamin D receptor and vitamin D ligands: two-dimensional alanine scanning mutational analysis. *Chem. Biol.* **10:** 261–270.
23. Ciesielski, F., N. Rochel, A. Mitschler, A. Kouzmenko, and D. Moras. 2004. Structural investigation of the ligand binding domain of the zebrafish VDR in complexes with 1alpha,25(OH)2D3 and Gemini: purification, crystallization and preliminary X-ray diffraction analysis. *J. Steroid Biochem. Mol. Biol.* **89–90:** 55–59.
24. Eelen, G., L. Verlinden, N. Rochel, F. Claessens, P. De Clercq, M. Vandewalle, G. Tocchini-Valentini, D. Moras, R. Bouillon, and A. Verstuyf. 2005. Superagonistic action of 14-epi-analogs of 1,25-dihydroxyvitamin D explained by vitamin D receptor-coactivator interaction. *Mol. Pharmacol.* **67:** 1566–1573.
25. Hourai, S., T. Fujishima, A. Kittaka, Y. Suhara, H. Takayama, N. Rochel, and D. Moras. 2006. Probing a water channel near the A-ring of receptor-bound 1 alpha,25-dihydroxyvitamin D3 with selected 2 alpha-substituted analogues. *J. Med. Chem.* **49:** 5199–5205.
26. Rochel, N., S. Hourai, X. Perez-Garcia, A. Rumbo, A. Mourino, and D. Moras. 2007. Crystal structure of the vitamin D nuclear receptor ligand binding domain in complex with a locked side chain analog of calcitriol. *Arch. Biochem. Biophys.* **460:** 172–176.
27. Rochel, N., J. M. Wurtz, A. Mitschler, B. Klaholz, and D. Moras. 2000. The crystal structure of the nuclear receptor for vitamin D bound to its natural ligand. *Mol. Cell.* **5:** 173–179.
28. Shimizu, M., Y. Miyamoto, H. Takaku, M. Matsuo, M. Nakabayashi, H. Masuno, N. Udagawa, H. F. DeLuca, T. Ikura, and N. Ito. 2008. 2-Substituted-16-ene-22-thia-1alpha,25-dihydroxy-26,27-dimethyl-19-norvita min D3 analogs: synthesis, biological evaluation, and crystal structure. *Bioorg. Med. Chem.* **16:** 6949–6964.
29. Tocchini-Valentini, G., N. Rochel, J. M. Wurtz, A. Mitschler, and D. Moras. 2001. Crystal structures of the vitamin D receptor complexed to superagonist 20-epi ligands. *Proc. Natl. Acad. Sci. USA.* **98:** 5491–5496.
30. Tocchini-Valentini, G., N. Rochel, J. M. Wurtz, and D. Moras. 2004. Crystal structures of the vitamin D nuclear receptor liganded with the vitamin D side chain analogues calcipotriol and seocalcitol, receptor agonists of clinical importance. Insights into a structural basis for the switching of calcipotriol to a receptor antagonist by further side chain modification. *J. Med. Chem.* **47:** 1956–1961.
31. Vanhooke, J. L., M. M. Benning, C. B. Bauer, J. W. Pike, and H. F. DeLuca. 2004. Molecular structure of the rat vitamin D receptor ligand binding domain complexed with 2-carbon-substituted vitamin D3 hormone analogues and a LXXLL-containing coactivator peptide. *Biochemistry.* **43:** 4101–4110.
32. Nakabayashi, M., S. Yamada, N. Yoshimoto, T. Tanaka, M. Igarashi, T. Ikura, N. Ito, M. Makishima, H. Tokiwa, H. F. DeLuca, et al. 2008. Crystal structures of rat vitamin D receptor bound to adamantyl vitamin D analogs: structural basis for vitamin D receptor antagonism and partial agonism. *J. Med. Chem.* **51:** 5320–5329.
33. Pace, C. N., F. Vajdos, L. Fee, G. Grimsley, and T. Gray. 1995. How to measure and predict the molar absorption coefficient of a protein. *Protein Sci.* **4:** 2411–2423.
34. Brunger, A. T., P. D. Adams, G. M. Clore, W. L. DeLano, P. Gros, R. W. Grosse-Kunstleve, J. S. Jiang, J. Kuszewski, M. Nilges, N. S. Pannu, et al. 1998. Crystallography & NMR system: a new software suite for macromolecular structure determination. *Acta Crystallogr. D Biol. Crystallogr.* **54:** 905–921.
35. McRee, D. E. 1999. XtalView/Xfit–a versatile program for manipulating atomic coordinates and electron density. *J. Struct. Biol.* **125:** 156–165.
36. Mi, L. Z., S. Devarakonda, J. M. Harp, Q. Han, R. Pellicciari, T. M. Willson, S. Khorasanizadeh, and F. Rastinejad. 2003. Structural basis for bile acid binding and activation of the nuclear receptor FXR. *Mol. Cell.* **11:** 1093–1100.
37. Inaba, Y., M. Nakabayashi, T. Itoh, N. Yoshimoto, T. Ikura, N. Ito, M. Shimizu, and K. Yamamoto. 2010. 22S-butyl-1alpha,24R-dihydroxyvitamin D3: recovery of vitamin D receptor agonistic activity. *J. Steroid Biochem. Mol. Biol.* **121:** 146–150.
38. Sato, H., A. Macchiarulo, C. Thomas, A. Gioiello, M. Une, A. F. Hofmann, R. Saladin, K. Schoonjans, R. Pellicciari, and J. Auwerx. 2008. Novel potent and selective bile acid derivatives as TGR5 agonists: biological screening, structure-activity relationships, and molecular modeling studies. *J. Med. Chem.* **51:** 1831–1841.

PEDS Advance Access published July 5, 2013

**Protein Engineering, Design & Selection** pp. 1–8, 2013
doi:10.1093/protein/gzt033

# Peptidyl-prolyl isomerase activity of FK506 binding protein 12 prevents tau peptide from aggregating

**Teikichi Ikura[1] and Nobutoshi Ito**

Laboratory of Structural Biology, Medical Research Institute, Tokyo Medical and Dental University, 1-5-45 Yushima, Bunkyo-ku, Tokyo 113-8510, Japan

[1]To whom correspondence should be addressed.
E-mail: ikura.str@tmd.ac.jp

**Received May 8, 2013; revised June 6, 2013; accepted June 16, 2013**

**Edited by Haruki Nakamura**

**The Alzheimer's disease-related protein, tau, aggregates into neurofibrillary tangles when it is hyperphosphorylated. The amino acid sequence included in the third repeat (R3) of the microtubule-binding region is suspected to be the main factor for tau aggregation. Here, we synthesized a 31-residue oligopeptide, corresponding to the R3 region, and characterized its aggregation propensity under various conditions. This peptide aggregated even in the absence of an aggregation-inducing molecule at a low salt concentration, while it did not form any aggregates at a high salt concentration. This suggests that hydrophilic interactions are the main cause of aggregation. We then investigated the function of FK506-binding protein (FKBP) 12, which is known to accumulate in neurofibrillary tangles *in vivo*, on aggregation of the R3 peptide and found that FKBP12 completely prevented the peptide from aggregating at a concentration ratio of 1 : 4 (peptide:FKBP12). FKBP12 also restored the oligomer of the peptide to its monomeric status. Mutational studies on the catalytic center of FKBP12 indicated that peptidyl-prolyl isomerase activity of FKBP12 was essential for prevention of aggregation. Assuming that the propensity of aggregation of the peptide is different in each *cis*-/*trans*-isomer, we propose that the aggregation behavior of the R3 peptide can be theoretically described with a simple kinetic scheme, in which only the *cis*-isomer can aggregate and FKBP12 catalyzes isomerization of the peptide in both the monomeric and aggregative states.**

*Keywords*: Alzheimer's disease/FK506 binding protein 12/neurofibrillary tangles/peptidyl-prolyl isomerase activity/tau protein

## Introduction

The tau protein is essential for assembly and stability of microtubule, which mainly consists of two types of tubulin (Weingarten *et al.*, 1975; Lindwall and Cole, 1984). Hyperphosphorylation of tau abolishes its ability to bind to tubulin and promote microtubule assembly (Bramblett *et al.*, 1993; Yoshida and Ihara, 1993). When it is released from tubulin, phosphorylated tau protein aggregates into neurofibrillary tangles (NFTs), which are the neuropathological hallmarks of Alzheimer's disease (AD) (Goedert *et al.*, 1988; Morishima-Kawashima *et al.*, 1995). Perez *et al.* (2001) showed that the microtubule-binding domain (MBD) of tau protein is involved in the core of NFT (Fig. 1). The ability to aggregate, however, was impaired in a variant of 3-repeat isoforms of tau protein, which lacked six residues Val306-Gln307-Ile308-Val309-Tyr310-Lys311, in the third region (R3), even though it was hyperphosphorylated. This suggests that the main factor for aggregation of tau protein is included in R3 (Perez *et al.*, 2007).

Dissection analysis was carried out for the MBD. Peptides corresponding to each of the four regions of the MBD (R1, R2, R3 and R4) and various combinations of these (R1–R3, R2–R3, R3–R4, R1–R2–R3, R1–R2–R3–R4 etc.) were chemically synthesized, and their aggregations were investigated by fluorescence-coupled circular dichroism and dynamic light scattering (Mizushima *et al.*, 2006; Zhou *et al.*, 2006; Sugino *et al.*, 2009). Only the peptides including R2 and/or R3 formed filaments in the presence of heparin, although their aggregation processes differed from each other.

A study in 1997 found that a peptidyl-prolyl isomerase (PPIase), Pin1, which specifically isomerized phosphorylated serine or threonine preceding a proline (pSer/Thr-Pro), restored the function of Alzheimer-associated phosphorylated tau protein (Yaffe, 1997; Lu *et al.*, 1999). Pin1 catalyzed prolyl isomerization of specific pSer/Thr-Pro motifs in tau protein to facilitate their dephosphorylation by a Pro-directed phosphatase, PP2A, which was conformation-specific and effectively dephosphorylated only the *trans*-pSer/Thr-Pro isomer (Zhou *et al.*, 2000). A high aggregation-prone (*cis*) isomer was converted to a low aggregation-prone (*trans*) isomer by PPIase activity of Pin1 (Nakamura *et al.*, 2012). As a result, the dephosphorylated tau protein regained ability for assembly and stability of microtubule (Zhou *et al.*, 2000). Phosphorylated sites were mapped on the sequences of various isoforms of tau protein (Brion *et al.*, 1993; Goedert *et al.*, 1993; Kopke *et al.*, 1993; Morishima-Kawashima *et al.*, 1995; Liu *et al.*, 2007). Pin1 worked on several specific sites of at least 30 phosphorylated sites (Lu *et al.*, 1999; Hamdane *et al.*, 2002; Smet *et al.*, 2004; Hamdane *et al.*, 2006; Landrieu *et al.*, 2010; Ogawa *et al.*, 2010). Phosphorylated Thr231-Pro232 was identified as the major target of Pin1 (Lu *et al.*, 1999; Zhou *et al.*, 2000; Nakamura *et al.*, 2012). No pSer/Thr-Pro motif, however, exists on the MBD, indicating that Pin1 does not directly affect the highest aggregation region of tau protein.

Recently, FK506-binding protein (FKBP) 12, FKBP51 and FKBP52 were found to bind to tau (Cao and Konsolaki, 2011). FKBPs are PPIases bound to FK506 and rapamycin (Siekierka *et al.*, 1989), and they generally show much higher PPIase activity on Xaa-Pro (Xaa; a standard amino acid residue) motifs than on pSer/Thr-Pro motif (Yaffe, 1997). Both of the large FKBPs, FKBP51 (51 kDa) and FKBP52 (52 kDa), are involved in tau turnover (Chambraud *et al.*, 2010; Jinwal *et al.*, 2010). Although FKBP51 and FKBP52 have very similar structure and both are mostly ubiquitously expressed, these proteins exert opposite effects on tau protein. FKBP51 promotes the association of tau protein with Hsp90, leading to

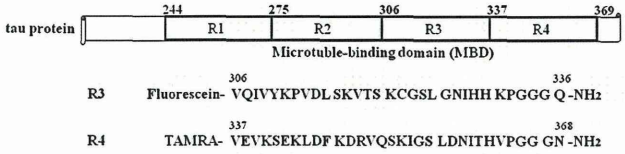


**Fig. 1.** Schematic diagram of four repeat regions in the microtubule-binding domain (MBD) of tau protein and amino acid sequences of the third and fourth repeats (R3 and R4). Labeled fluorophores used in the present study are also shown to the left of the sequences.

dephosphorylation and proper recycling of tau protein (Jinwal *et al.*, 2010), whereas FKBP52 binds directly and specifically to tau protein, preventing tau protein from binding to tubulin (Chambraud *et al.*, 2010). On the other hand, the smaller FKBP12 (12 kDa) co-localized with NFT in AD brains, suggesting that FKBP12 interacted with abnormal forms of tau protein (Harding *et al.*, 1989; Sugata *et al.*, 2009). It is possible that FKBP12 interacts with the MBD of tau protein because the MBD contains eight Xaa-Pro motifs. Assuming each *cis*-/*trans*-isomer of the Xaa-Pro motif in the MBD corresponds with the normal or abnormal form of tau, as seen for phosphorylated Thr231-Pro232, FKBP12 might be able to restore abnormal forms of tau protein to its normal forms. Thus, FKBP12 is a candidate to regulate tau protein by interacting with its MBD.

Here, we synthesized a peptide that corresponds to the R3 region of tau protein (R3 peptide) and investigated whether or not FKBP12 prevents its aggregation *in vitro* under various conditions by fluorescence and dynamic light scattering measurements. In the present study, we focused on the early stage of aggregation of the R3 peptide because Pin1 affected tau protein at the early stage of aggregation (Ramakrishnan *et al.*, 2003; Nakamura *et al.*, 2012). The early stage of aggregation, however, is poorly understood, particularly because of the difficultly of its detection. Thus, we labeled the R3 peptide with fluorescein to increase sensitivity. First, we checked if fluorescein did not change the nature of the peptide with respect to aggregation and investigated the aggregation mechanism for the R3 peptide by measuring aggregation under various conditions. We then measured the aggregation of the R3 peptide in the presence of FKBP12 in order to investigate the aggregation inhibitory activity of FKBP12. As a result, higher the concentration of FKBP12 became, less the aggregation of the R3 peptides was detected. Next, we investigated the aggregation inhibitory mechanism by FKBP12 by introducing two types of mutations Val55 → Arg and Tyr82 → Lys. The former mutation increased the activity 11-fold, whereas the latter decreased it 7-fold. We globally analyzed the relationship between the PPIase activity of FKBP12 and the aggregation inhibitory activity. On the basis of these results, we concluded that the PPIase activity of FKBP12 prevented the R3 peptide from aggregating.

## Materials and methods

### *Chemicals*

Heparin sodium was of Wako Special Grade from Wako Pure Chemical Industries Ltd. All other chemicals were of guaranteed reagent grade.

### *Peptides and proteins*

The R3 and R4 peptides, the sequences of which are shown in Fig. 1, were chemically synthesized using a solid-phase peptide synthesizer (Sigma Aldrich Japan K.K.). A fluorescein and an amide group were attached to the N-terminal amide group of Val1 and the C-terminal carboxyl group of Glu31 in the R3 peptide, respectively. TAMRA and amide group were attached to the N-terminal amide group of Val1 and the C-terminal carboxyl group of Asn32 in the R4 peptide, respectively. Their purity was 94.4 and 98.7% for the R3 and R4 peptides, respectively, as determined by mass spectrometry. These peptides were obtained in lyophilized form.

Wild-type human FKBP12 and its two mutants, FKBP12/Val55Arg and FKBP12/Tyr82Lys, were expressed and purified as described previously (Ikura and Ito, 2007).

### *Time-dependent fluorescence measurement*

Aggregation of the R3 peptide quenched the fluorescence of fluorescein attached to the peptide; as the peptide became more aggregated, the change in fluorescence intensity became larger, as shown in Fig. 2a. Therefore, time-dependent change in fluorescence intensity by fluorescein was measured by a JASCO FP-6500 spectrofluorometer to monitor the time-course of aggregation of the R3 peptide. The excitation and emission wavelengths were 450 and 520 nm, respectively. Before measurements were taken, 1500 μl of each buffer solution including salt, heparin, reducing agent or FKBP12, was pre-incubated at 25°C in a rectangular optical cell settled in a Peltier thermostatted cell holder with a magnetic stirrer. Aggregation of the R3 peptide was initiated by diluting 1.5 μl of 5 mM (or 15 μl of 0.5 mM) of the R3 peptide dissolved in 100% dimethyl sulfoxide (DMSO) in the optical cell. Fluorescence intensity was recorded with time intervals from 5 min to 4–60 h after mixing the peptide. On the other hand, we measured time-dependent change in fluorescence intensity by TAMRA to monitor time-course of aggregation of the R4 peptide as a control experiment. The excitation and emission wavelengths were 500 and 575 nm, respectively. The other experimental conditions and procedures for the R4 peptide were the same as those for the R3 peptide.

### *Fluorescence depolarization measurements*

The fluorescence depolarization of fluorescein attached to the R3 peptide was measured by the Peltier thermostatted depolarization accessory settled on JASCO FP-6500 spectrofluorometer to investigate the interaction between the R3 peptide and FKBP12 (Weber, 1953; Lakowicz, 1983). The excitation and emission wavelengths were 450 and 520 nm, respectively. Before measurements, 1500 μl of each buffer solution including appropriate amount of FKBP12 was pre-incubated at 25°C in a rectangular optical cell settled in the Peltier thermostatted cell holder with a magnetic stirrer. Then, 3 μl of 0.5 mM of the R3 peptide solved in 100% DMSO was diluted in the solution. The final concentration of the peptide was set to 1 μM, because aggregation of the peptide was not detected at this concentration. Fluorescence depolarization was measured at least 20 times for each condition, and then averaged. These measurements gave apparent dissociation constants ($K_d$) averaged for both of the *cis*- and *trans*-isomers.

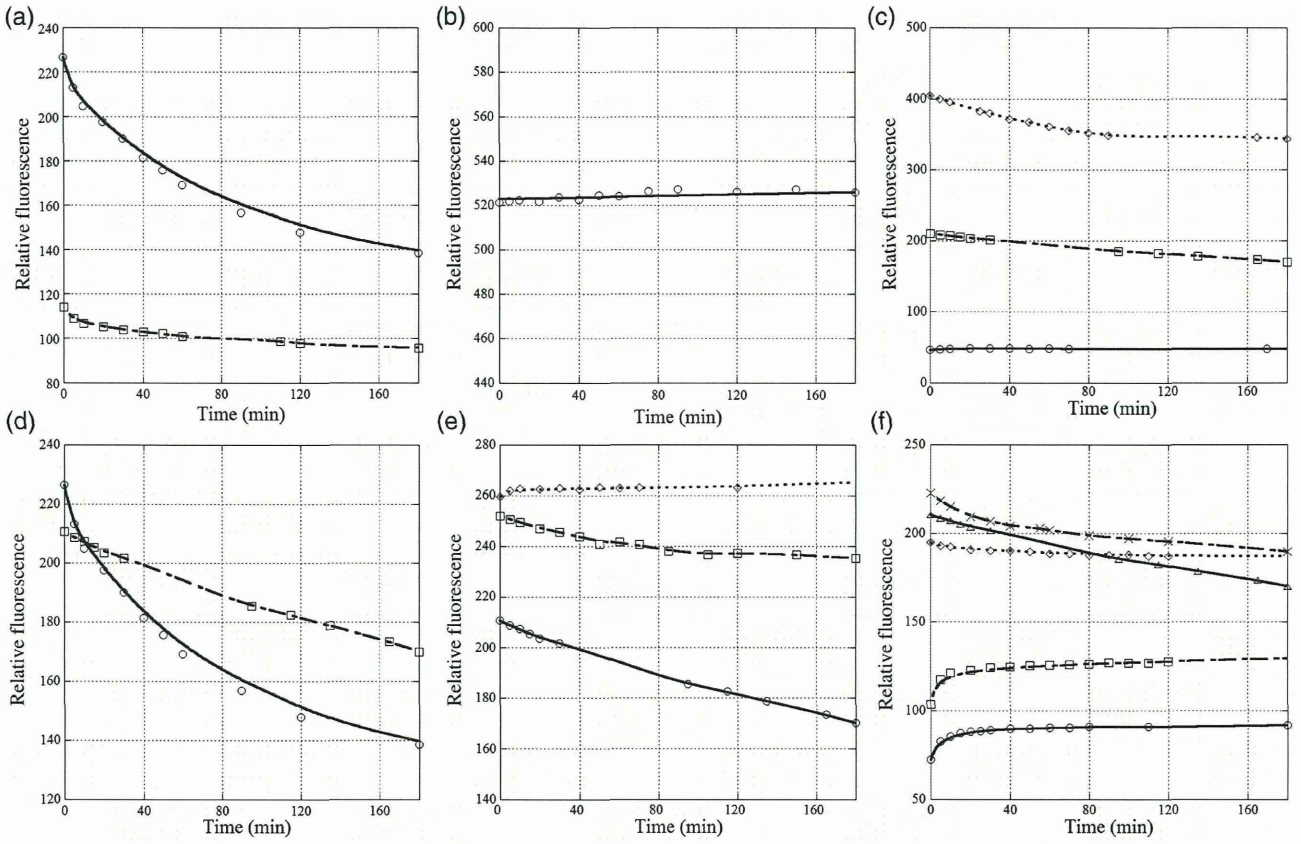


**Fig. 2.** Aggregation of the R3 and R4 peptides under various conditions. Aggregation of the R3 and R4 peptides was monitored in 50 mM sodium phosphate buffer at 25°C with the relative fluorescence of fluorescein and TAMRA attached to the N-terminal amide group of the peptides, respectively. The reaction was started by diluting a 5-mM stock solution of the peptides 1000 times. The other conditions are described in each panel. (**a**) The aggregation of 5 μM of the R3 peptide at pH 8.0 in the absence (empty circle) and presence (empty square) of 60 μg/mL heparin. (**b**) The aggregation of the R4 peptide in the absence of heparin. (**c**) The aggregation of 1 μM (empty circle), 5 μM (empty square) and 10 μM (empty rhombus) of the R3 peptide at pH 8.0 in the presence of 10 mM tris-(2-carboxyethyl)-phosphine hydrochloride (TCEP). (**d**) The aggregation of 5 μM of the R3 peptide at pH 8.0 in the absence (empty circle) and presence (empty square) of 10 mM TCEP. (**e**) The aggregation of 5 μM of the R3 peptide at pH 8.0 in the presence of 10 mM TCEP, and in 0 (empty circle), 100 (empty square) or 400 (empty rhombus) mM sodium chloride. (**f**) The aggregation of 5 μM of the R3 peptide in the presence of 10 mM TCEP, and at pH 4.5 (empty circle), 5.9 (empty square), 6.9 (empty rhombus), 8.0 (empty triangle) or 9.4 (multiplication sign). The aggregation of 5 μM of the R3 peptide at pH 8.0 in the presence of 10 mM TCEP was redundantly plotted in the panels (c), (d), (e) and (f) as a control data. The curve fitting was performed by applying a Stineman interpolating function to the data on KaleidaGraph (Hukinks).

### *Dynamic light scattering measurement*

Aggregation of the R3 and R4 peptides were directly monitored at 25°C by dynamic light scattering method using Marvern Zetasizer μV. During aggregation measurement, we collected 4 μl of the reaction mixture at hourly intervals and measured ingredient size in the mixture by a laser beam of 830 nm at an angle of 90°.

### *Numerical analysis*

Numerical analyses were performed using the Mathematica 9.0 software package (Wolfram Res.).

## Results

### *Characterization of the R3 peptide's aggregation*

To characterize aggregation of the R3 region of tau protein, we chemically synthesized the R3 peptide, the N-terminal valine of which was labeled with fluorescein (Fig. 1), and investigated its aggregation under various conditions by change in the fluorescence intensity of fluorescein. Aggregation of tau protein and peptides has been conventionally monitored with thioflavin-S (ThS), which quantitatively associates with their aggregated forms. However, it was recently revealed that ThS itself increased the amount of aggregation of tau protein (Carlson *et al.*, 2007; Perez *et al.*, 2007). Thus, we directly labeled the tau peptide with fluorescein to monitor its aggregation in order to exclude ThS-induced artifacts.

*Inducer.* Polyanionic compounds, such as heparin, are well known as *in vitro* inducers for aggregation of the R3 peptide, as well as the tau protein, although the physiological inducer for NFT is not known (Carlson *et al.*, 2007). Initially, we determined whether or not heparin had a similar effect on aggregation of the labeled R3 peptide, because no experimental data have been reported for the labeled R3 peptide (Fig. 2a). As reported for the non-labeled peptides (Mizushima *et al.*, 2006), 5 μM of the labeled R3 peptide rapidly aggregated in the presence of 60 μg/ml of heparin, and then its aggregates gradually grew into larger particles. We also found that the peptide aggregated at this concentration even in the absence of heparin (Fig. 2a). The aggregation in the absence of heparin,